Dalton Transactions

Cite this: *Dalton Trans.*, 2011, **40**, 9474

www.rsc.org/dalton

PAPER

New 2,3-disubstituted-5-hydroxyquinoxaline ligands and their coordination chemistry with cyclometallated iridium(III): syntheses, structures and tunable electronic properties†

Andrew J. Hallett,* Benson M. Kariuki and Simon J. A. Pope*

Received 19th April 2011, Accepted 5th July 2011
DOI: 10.1039/c1dt10707k

A new series of *para*-substituted 2,3-diphenyl-5-hydroxyquinoxaline ligands (**LH^n**) were synthesised and characterised. These ligands were prepared in high yield *via* a two-step synthetic method. Four novel heteroleptic iridium(III) complexes were correspondingly prepared in high yield giving [**Ir(ppy)$_2$(L^n)**]. Two X-ray crystallographic studies were undertaken on **LH^3** and [**Ir(ppy)$_2$(L^2)**] with each confirming the proposed formulations, with the complex showing the O,N-coordination mode of the quinoxalinato ligand. Density functional theoretical calculations were performed, firstly to compare the coordinated quinoxalinato system with the related quinolinato analogue, and secondly to probe the influence of the variation in *para*-substitution on the ancillary ligand. The calculations suggest that for either the quinoline or quinoxaline systems ligand-centred character appears to dominate the HOMO and LUMOs. Experimental electrochemical and spectroscopic characterisation showed that the subtle variations in absorption and emission wavelengths are probably due to ligand-dominated transitions that are influenced by the electronic nature of the *para*-substituted phenyl units in coordinated **L^n**.

Introduction

Whilst there have been numerous reports on metal ion complexes (for example Al(III), B(III) and Pd(II))[1] containing commercially available 8-hydroxyquinoline derivatives, only a few describe the incorporation of substituted hydroxyquinoline ligands into iridium(III) complexes.[2] Given the recent and rapid development of Ir(III) complexes towards a variety of opto-electronic related applications such as OLEDs,[3] electrochemical cells (LECs),[4] photovoltaic[5] and luminescent imaging applications,[6] hydroxyquinoline ligands and related systems may offer useful avenues for future applications. The ability to easily tune the optical properties of Ir(III) complexes *via* the use of ancillary ligands is therefore of great general value. In the specific case of hydroxyquinoline species the ligand-centred excited state character can be tuned through a detailed appreciation of the IL(phenol-to-pyridine)CT transition.[7] The accepting ability (*i.e.* the LUMO energy) of the pyridine ring is particularly sensitive to substitution at the 5-position.[8] In this manner, modulation of the electronic character at the 5-position can conveniently tune the absorption and emission profiles of the ligand and resultant complexes based on Al(III) and Ir(III) (Fig. 1). In the case of the *bis*-cyclometalled Ir(III) complexes the electronic nature of the ancillary hydroxyquinoline ligand determines the extent of the LUMO localisation on that ligand.[9]

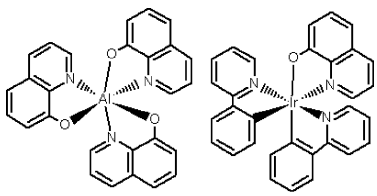

Fig. 1 The structures of [AlQ_3] and [$Ir(py)_2Q$].

In light of this, we have developed a range of related 5-hydroxyquinoxaline ligands that are easily substituted with various aryl units. Our theoretical studies suggest that the LUMO of these ligands can be more effectively localised upon the hydroxyquinoxaline unit. As a consequence, the corresponding Ir(III) complexes demonstrate some tunable behaviour with respect to their luminescent properties.

Here we report a new, convenient procedure for the synthesis of functionalised 5-hydroxyquinoxaline species, yielding three new ligands **LH^2**, **LH^3** and **LH^4** with substituents of varied electronic character in the 2,3-positions of the pyrazine ring. Together with the known ligand **LH^1**, we describe their coordination chemistry with a *bis*-cyclometallated Ir(III) precursor, giving the first examples of neutrally charged, heteroleptic Ir(III) complexes containing functionalised quinoxalinato-based ligands.

School of Chemistry, Main Building, Cardiff University, Cardiff, CF10 3AT. E-mail: popesj@cardiff.ac.uk, hallettaj@cardiff.ac.uk; Fax: (+44) 029-20874030; Tel: (+44) 029-20879316

† CCDC reference numbers 822159 and 822160. For crystallographic data in CIF or other electronic format see DOI: 10.1039/c1dt10707k

The syntheses, selected structures and spectroscopic properties of the ligands and complexes are reported herein.

Results and discussion

Synthesis and characterisation

Four *para*-substituted 2,3-diphenyl-5-hydroxyquinoxaline ligands, **LH$^{1-4}$** (1 = *p*-H, 2 = *p*-Br, 3 = *p*-Me, 4 = *p*-OMe), were prepared in a simple two-step reaction procedure (Scheme 1). First, 2-amino-3-nitrophenol was reduced by heating to reflux in acidic EtOH for 14 h in the presence of zinc dust, giving the corresponding 2,3-diamino species. Subsequent condensation with a range of substituted diones in refluxing EtOH for 16 h gave the desired ligands, and for **LH^{1}**, **LH^{3}** and **LH^{4}**, without recourse to further purification. Column chromatography (silica, CH_2Cl_2) was, however, required for the purification of **LH^{2}**: all of the ligands were isolated in high yields (82–100%). Although **LH^{1}** has been previously reported, these did not include full spectroscopic characterisation, which are therefore included here for clarity and comparison.[10]

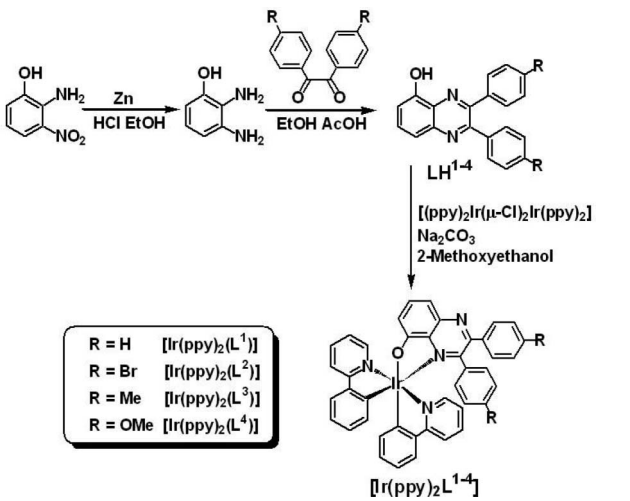

Scheme 1 Synthetic route to ligands **LH^{n}** and complexes **[Ir(ppy)$_2$L^{n}]** (*n* = 1–4).

The ligands were each characterised using ^{1}H and ^{13}C{^{1}H} NMR spectroscopy, mass spectrometry and electronic spectroscopy. The distinguishing features of the ^{1}H NMR studies revealed characteristic resonances associated with the quinoxaline-appended *para*-substituted phenyl groups. For example, **LH^{2}** (the *para*-Br derivative) gave two signature multiplet resonances at 7.44 and 7.30 ppm, attributed to the phenyl groups, observed upfield from the starting dione precursor (*cf.* 7.77 and 7.60 ppm in $CDCl_3$). In all four ligands the proton resonances of the quinoxaline unit are perturbed by the subtle electronic changes imposed by the substituted phenyl groups, suggesting an element of electronic communication throughout the ligand and quinoxaline unit. ES$^+$ mass spectrometry revealed the protonated parent ions [M+H]$^+$ for **LH^{1}**, **LH^{2}** and **LH^{4}**, whereas EI showed the parent ion [M]$^+$ for **LH^{3}**. The ligand **LH^{3}** was also characterised by X-ray crystallography (see X-ray crystallography section).

The neutrally charged hetero-ligand complexes **[Ir(ppy)$_2$L^{n}]** (*n* = 1–4) were isolated following addition of base to a reaction mixture composition of 2 : 1 ligand to [(ppy)$_2$Ir(μ-Cl$_2$)Ir(ppy)$_2$] in 2-methoxyethanol, in excellent yields of 88–96 %. The complexes were characterised in the solution state using ^{1}H and ^{13}C{^{1}H} NMR, UV-vis. and luminescence spectroscopies. Due to the unsymmetrical nature of the quinoxaline ligands, rendering the phenylpyridine ligands inequivalent, the ^{1}H and ^{13}C{^{1}H} NMR spectra were very complex. For example, **[Ir(ppy)$_2$L^{1}]** showed 38 unique resonances in the aromatic region of the ^{13}C{^{1}H} NMR spectrum. ES mass spectrometry (including HR) revealed the protonated parent ions [M+H]$^+$ for each complex.

Table 1 Parameters associated with the single crystal diffraction data collection for **LH^{3}** and **[Ir(ppy)$_2$(L^{2})]**

	LH^3	[Ir(ppy)$_2$(L^2)]·0.85Et$_2$O
Formula	$C_{22}H_{18}N_2O$	$C_{44.4}H_{33.8}Br_2IrN_4O_2$
Formula weight	326.38	1007.37
T/K	150(2)	150(2)
Wavelength/Å	0.71073	0.71073
Crystal system	Monoclinic	Monoclinic
Space group	$P2_1/n$	$P2_1/n$
a/Å	13.9500(4)	18.3163(6)
b/Å	16.8880(5)	9.7199(4)
c/Å	15.3970(4)	23.3380(5)
α/°	90.00	90.00
β/°	102.071(2)	110.101(2)
γ/°	90.00	90.00
Volume/Å^3	3547.14(17)	3901.84(20)
Z	8	4
F000	1376	1965
μ/mm^{-1}	0.076	5.513
Reflections collected	14775	16143
Independent reflections (R_{int})	8077 (0.0642)	8941 (0.0782)
Final $R1$ [$I > 2\sigma(I)$]: R_1, wR_2	0.0705, 0.1390	0.0692, 0.1217

Table 2 Selected bond lengths (Å) and angles (°) for **[Ir(ppy)$_2$(L^{2})]** and the values calculated from DFT studies

Bond length (Å)/angle (°)	[Ir(ppy)$_2$(L^2)]	Calculated values
Ir(1)–N(1)	2.232(7)	2.310
Ir(1)–N(3)	2.036(7)	2.052
Ir(1)–N(4)	2.040(7)	2.039
Ir(1)–O(1)	2.132(5)	2.150
Ir(1)–C(1)	1.996(8)	1.996
Ir(1)–C(2)	1.991(8)	2.008
O(1)–Ir(1)–N(1)	78.1(2)	76.6
N(1)–Ir(1)–N(3)	95.2(3)	93.0
N(3)–Ir(1)–N(4)	173.7(3)	174.6

X-ray crystallography

Single crystals suitable for X-ray diffraction studies were isolated using vapour diffusion of Et_2O in to $CHCl_3$ solutions of the ligand or complex over a period of 24 h at room temperature. The parameters associated with the data collection are presented in Table 1 with selected bond lengths and angles (principally involving the coordination sphere of **[Ir(ppy)$_2$(L^{2})]**) shown in Table 2.

The solid-state structural determination of **LH^{3}** confirmed the formation of the quinoxaline ligand (Fig. 2, Table 1) showing that both tolyl groups are twisted out of the plane of the quinoxaline unit, presumably to minimise steric repulsions.

The structural analysis of **[Ir(ppy)$_2$(L^{2})]** also supports the proposed formulation determined from solution state spectroscopic

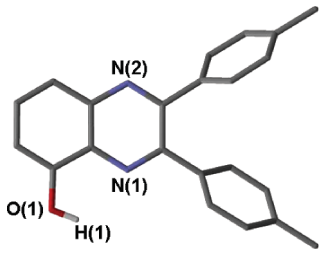

Fig. 2 The structure of **LH**[3]. All hydrogen atoms other than H(1) are omitted for clarity.

analyses (Fig. 3, Tables 1 and 2). The complex possesses pseudo-octahedral coordination geometry, with a chelated quinoxalinato derivative bound through the oxygen and nitrogen donor atoms. As with numerous related examples of this type, the relative coordination geometry of the cyclometallated phenylpyridine ligands is retained from that of the precursor (*i.e. cis* C,C and *trans* N,N).[11] From a steric perspective, it is noted that the 2-substituted *para*-BrC_6H_4 group is twisted close to orthogonality in an effort to minimise clashes with the coordinated phenylpyridine ligand.

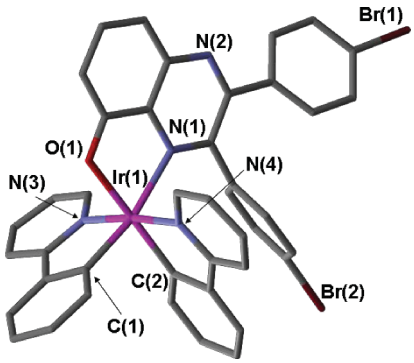

Fig. 3 The structure of [**Ir(ppy)$_2$(L^2)**]. Hydrogen atoms and solvent molecules are omitted for clarity.

The bond lengths and angles of [**Ir(ppy)$_2$(L^2)**] were compared with the optimised values calculated from density functional theory (DFT) (Table 2). In general, a reasonable agreement is obtained between the theoretical and experimentally observed bond lengths, although some small differences are found. The optimised Ir–C bond lengths are slightly different with Ir–C(1) (1.996 Å) shorter than Ir–C(2) (2.008 Å) conflicting with the experimental data. In the case of the Ir–O bonds, the calculated value is 2.150 Å, which is longer by 0.018 Å than the value obtained by X-ray crystallography; similarly the Ir–$N_{quinoxaline}$ bond, where the calculated value is 0.078 Å longer.

Density functional theory (DFT) studies

In an effort to elucidate the nature of the electronic transitions within this class of complex, DFT calculations (computed using the B3PW91 hybrid orbital) were undertaken. In these examples, an assessment of the frontier orbitals provided a qualitative insight into the HOMO (highest occupied molecular orbital) and LUMO (lowest unoccupied molecular orbital) energy levels.

Firstly, it is noteworthy that here, as in previous studies,[12] the HOMO of the related 8-hydroxyquinoline complex [**Ir(ppy)$_2$Q**] is located primarily on the metal and ancillary ligand (Fig. 4). The

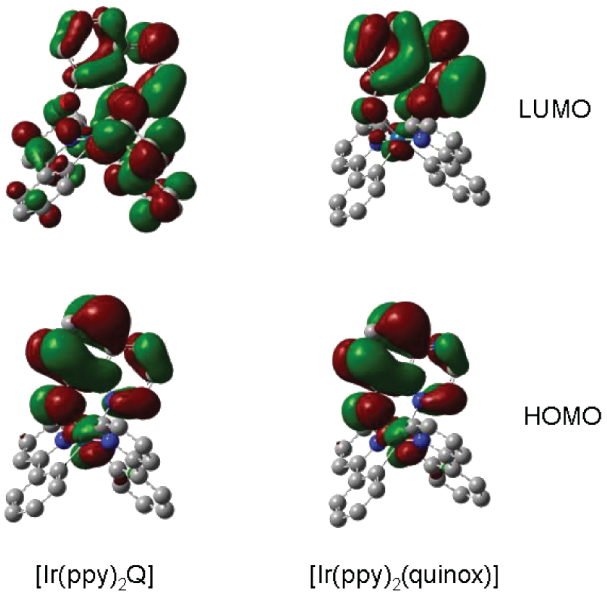

Fig. 4 Graphical representation of the frontier orbitals of [**Ir(ppy)$_2$Q**] and [**Ir(ppy)$_2$(quinox)**].

HOMO is distributed over the whole of the quinoline ligand, with no electron density located on the cyclometallated phenylpyridine ligands. The LUMO entails distribution over the metal centre and ancillary quinoline ligand, with additional coverage on the cyclometallated phenylpyridine ligands.

Replacing the quinolinato moiety with quinoxalinato gives the reference compound [**Ir(ppy)$_2$(quinox)**], wherein the HOMO remains essentially unchanged. Importantly, the LUMO is predicted on the metal centre and ancillary ligand, with little or no contribution from the cyclometallated ligands (Fig. 4). These results therefore suggest that appropriate functionalisation of 5-hydroxyquinoxaline ligands could feasibly yield tunable optical characteristics within the corresponding Ir(III) complexes.

For the quinoxalinato complexes described here the energy levels of both the HOMO and LUMO are sufficiently different ($\Delta E > 0.2$ eV) from the other MOs to be considered independent. As with the unsubstituted [Ir(ppy)$_2$(quinox)], both the HOMO and LUMO are located primarily on the quinoxaline ligand and the metal 5d(Ir) centre (Fig. 5). Population analyses (Table 3) revealed that the distribution of the frontier orbitals over the various ligands and metal is very similar in each case for [Ir(ppy)$_2$L^n] (HOMO: 15.2–16.3% Ir; 77.6–78.9% L^n; 2.1–2.2% ppy *trans* to N; 3.7–4.2% ppy *trans* to O. LUMO: 1.8–1.9% Ir; 94.0–95.2% L^n; 1.5–2.2% ppy *trans* to N; 1.3–2.0% ppy *trans* to O). Although there is no direct contribution from the substituted phenyl rings to the HOMO coverage, the nature of the *para*-substituent does appear to impart an influence on the overall energy level. In contrast, the LUMO is partially delocalised over the substituted phenyl rings. Of course, due to relativistic effects, absolute energy levels cannot be reliably calculated for complexes of heavy metal ions, but relative energy levels can still be informative. For example, the complex of the electron withdrawing *para*-Br ligand [**Ir(ppy$_2$)L^2**] has the lowest HOMO energy level ($E = -5.03$ eV) whereas the complex of the electron donating *para*-OMe has the highest ($E = -4.73$ eV). Similarly, the LUMO energies also reflect this variation (*para*-Br $E_{LUMO} = -2.12$ eV; *para*-OMe $E_{LUMO} = -1.74$ eV). Again,

Table 3 Percentage distribution of HOMO and LUMO in $[\mathbf{Ir(ppy)_2L^n}]$ (n = 1–4)

	$[Ir(ppy)_2L^1]$		$[Ir(ppy)_2L^2]$		$[Ir(ppy)_2L^3]$		$[Ir(ppy)_2L^4]$	
	HOMO	LUMO	HOMO	LUMO	HOMO	LUMO	HOMO	LUMO
Ir	16.0	1.9	16.3	1.9	15.3	1.8	15.2	1.8
L^n	78.1	94.7	77.6	95.2	78.4	94.2	78.9	94.0
ppy 1	2.2	1.8	2.2	1.5	2.1	2.1	2.1	2.2
ppy 2	3.7	1.7	3.8	1.3	4.2	1.9	3.8	2.0

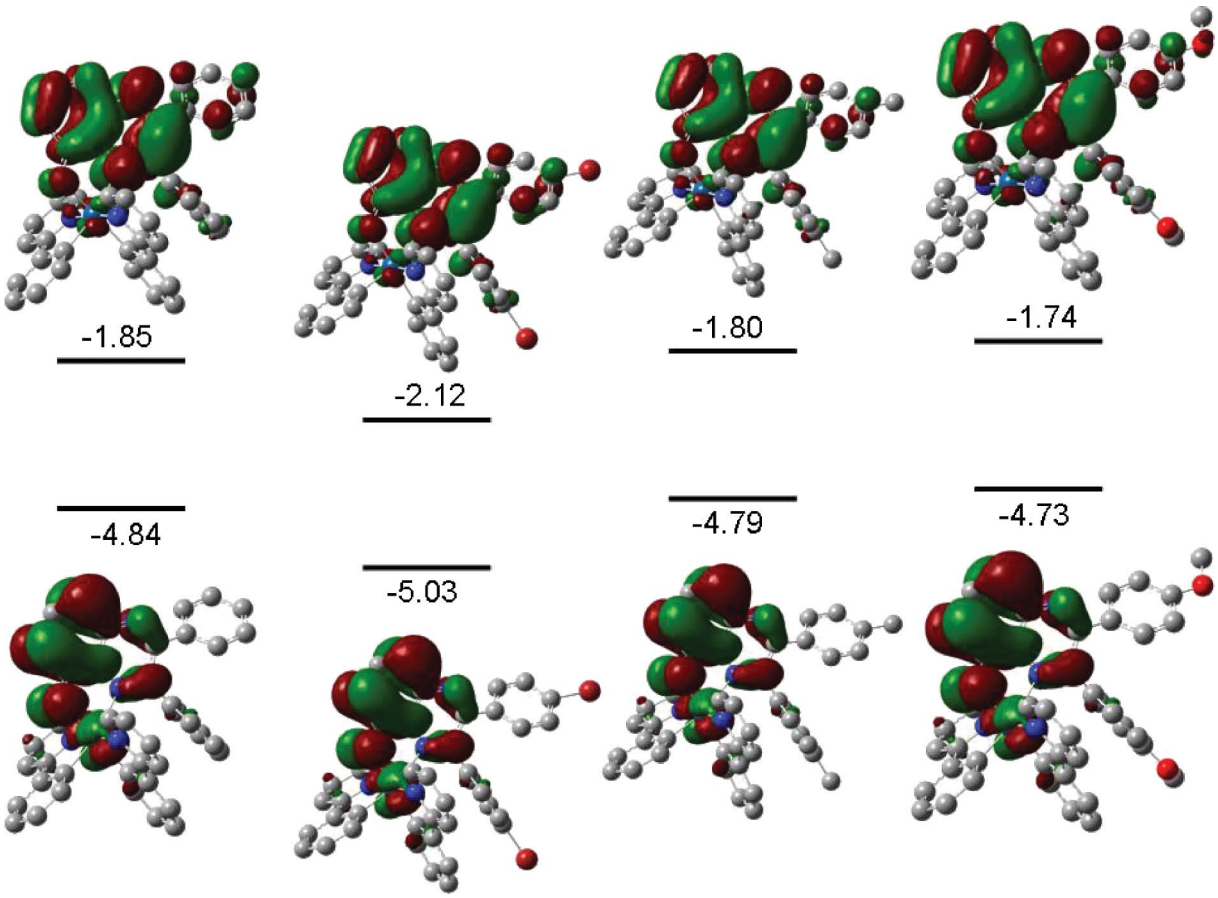

Fig. 5 Graphical representation of the frontier orbitals of $[\mathbf{Ir(ppy)_2L^n}]$ (n = 1–4 left to right). Bottom, HOMO; top, LUMO.

this calculated data suggests that variation of the remote *para* substituent can lead to a degree of tunable optical properties within this series of complexes. Interestingly, the calculated HOMO–LUMO bandgaps do not vary a great deal (2.91–2.99 eV).

Electrochemical studies

An investigation into the electrochemical behaviour of the four complexes was undertaken in de-aerated CH_2Cl_2. Electrochemical studies were performed in order to approximate the HOMO energy levels for each complex, since the ionisation potential for the first oxidation can be used to establish E_{HOMO} assuming that the absolute level of the $FeCp_2^{0/1+}$ redox couple is 4.8 eV below the vacuum level. The cyclic voltammograms, measured at a platinum disc electrode (scan rate 200 mV s^{-1}, 1×10^{-3} M solutions, 0.1 M NBu_4PF_6 as a supporting electrolyte) of the complexes $[\mathbf{Ir(ppy)(L^n)}]$ (n = 1–4) each showed one or two oxidations, which were not fully reversible (Table 4). Each complex also showed an irreversible reduction wave close to the edge of the solvent window.

The first oxidation potential varies very little across the series of complexes (0.87–0.90 V): the difference in oxidation potentials is presumably due to the subtle donor variations of the substituted quinoxalinato ligands. The E_{HOMO} values were calculated using the reported equations[13] and the resultant values, ranging from –5.20 to –5.23 eV, are detailed in Table 4.

Spectroscopic properties of the ligands and complexes

The UV-vis absorption spectra of the ligands and complexes were measured as aerated MeCN solutions. The absorption properties of the ligands are dominated by a broad visible absorption around 320–410 nm attributed to IL transitions, possibly including phenol-to-pyrazine charge transfer. The electronic nature of the *para*-substituted groups subtly influences the positioning of this absorption band. Indeed, the relatively electron poor Ph and

Table 4 Absorption, emission and electrochemical properties of the free ligands and corresponding iridium complexes

Ligand/Complex	λ_{max} (ε/M^{-1}cm^{-1})/nm[a]	E_{ox}/V[b]	HOMO/eV[c]	$E_{bandgap}$/eV[d]	LUMO/eV[e]	λ_{em}/nm[f]	τ (ns) aerated[f]	Φ_{em} [f,h]
LH^1	289(19600), 350(6200)	—	—	—	—	459	5.5	—
LH^2	294(16950), 349(5100)	—	—	—	—	473	7.8	—
LH^3	292(16450), 355(7050)	—	—	—	—	474	3.0	—
LH^4	297(20000), 364(9200)	—	—	—	—	438	5.3	—
[Ir(ppy)$_2$(L^1)]	302(18050)	0.87	−5.20	1.83	−3.37	462	5.0	0.010
[Ir(ppy)$_2$(L^2)]	302(16650)	0.89	−5.22	1.83	−3.39	436	6.7[g]	0.008
[Ir(ppy)$_2$(L^3)]	294(14450)	0.88	−5.21	1.83	−3.38	456	4.4	0.013
[Ir(ppy)$_2$(L^4)]	286(14450)	0.90	−5.23	1.83	−3.40	503	4.9	0.019

[a] Absorption spectra measured as MeCN solutions (6.4×10^{-5} mol dm^{-3}). [b] Oxidation potentials measured as CH_2Cl_2 solutions at 200 mVs^{-1} with 0.1 M $[NBu_4][PF_6]$ as supporting electrolyte calibrated with Fc/Fc$^+$. [c] The HOMO energy level was calculated using the equation HOMO (eV) = E_{ox} − $E_{Fc/Fc+}$ + 4.8. [d] $E_{bandgap}$ was determined from the absorption edge of the iridium complexes. [e] The LUMO energy level was calculated using the equation LUMO (eV) = HOMO + $E_{bandgap}$. [f] Excitation at 372 nm. [g] Excitation at 295 nm. [h] Estimated errors of ±15%.[16]

para-Br substituted ligands, **LH^1** and **LH^2**, respectively, possess similar absorption maxima (~350 nm), whereas the electron-donating *para*-OMe substituted ligand, **LH^4**, showed a significant bathochromic shift (364 nm) together with an increase in molar absorption coefficient (Table 4). In addition, the bands at 289–297 nm are assigned to purely intra-ligand π–π* transitions for each example.

The complexes all absorb in the visible region (Fig. 6, Table 4): the features are in the range 250–600 nm and are typically broad in appearance. The complexes each exhibit a relatively weak absorption band that tails into the visible region, assigned to spin allowed (singlet) and possibly spin forbidden (triplet) metal-to-ligand charge transfer (MLCT) transitions, together with superimposed perturbed ligand-centred bands. Significantly stronger absorption bands resulting from ligand-centred π–π* transitions are observed in the higher energy region around 300 nm.

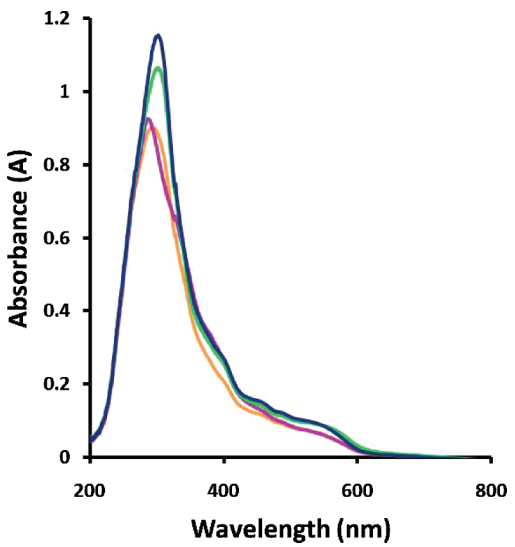

Fig. 6 UV-vis spectra of **[Ir(ppy)$_2$L^1]** (blue), **[Ir(ppy)$_2$L^2]** (green), **[Ir(ppy)$_2$L^3]** (orange) and **[Ir(ppy)$_2$L^4]** (pink) as MeCN solutions (6.4×10^{-5} M).

Luminescence measurements were conducted on MeCN solutions using a 372 nm excitation (Table 4). Firstly, the free ligands display a short-lived (τ = < 10 ns) fluorescence, which appeared as a broad band in the visible region (*ca.* 440–480 nm). As with the related hydroxyquinoline chromophores, it is reasonable to assume that this is dominated by an IL ^{1}π–π* transition. The subtleties associated with the emission wavelengths of the ligands can, in part, be attributed to the electronic influence of substitution in the *para* position of the aryl units. For example, the methoxy derivative, **LH^4**, possesses the highest energy emission wavelength.

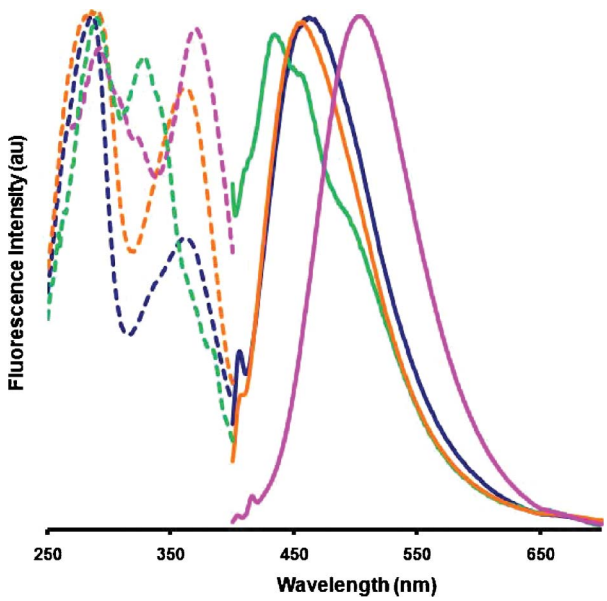

Fig. 7 Excitation (dashed) and emission (solid) spectra of **[Ir(ppy)$_2$(L^1)]** (blue), **[Ir(ppy)$_2$(L^2)]** (green), **[Ir(ppy)$_2$(L^3)]** (orange) and **[Ir(ppy)$_2$(L^4)]** (pink). λ_{ex} = 372 nm.

The photophysical data for the complexes is also presented in Table 4 and shows that the nature of the emission from the complexes is probably dominated by ligand(quinoxalinato)-centred character (see Fig.7). When compared to the free ligands, the emission wavelengths and lifetimes of the complexes suggest a metal-perturbed, ligand-dominated emissive state. The low quantum yields are also consistent with such an assignment since in aerated solvent the iridium centre would be expected to assist non-radiative deactivation of the ligand-centred excited states. This contrasts with related reports on quinolinato complexes of iridium: such complexes are not uniformly emissive (attributed to unfavourable mixing of singlet and triplet excited states), but those that are show some weak phosphorescence in degassed

solvent.[14] Related quinolinato complexes of Al(III) have shown that there is also significant CT character that originates from intraligand phenolate-to-pyridine transitions.[8b] Our DFT studies suggest that a similar electronic character is inherent within the Ir complexes described here. The calculations propose that the HOMO in each case comprises significant phenolate character, together with some Ir-centred orbital contributions; in each case the LUMO has significant pyrazine-localised electron density.

Experimentally, a clear trend is evident in the complexes whereby an electron-withdrawing group (**L²**) blue-shifts the emission peak, but an electron donating group red-shifts (**L⁴**). The wavelength variations within this series, demonstrates an ability to tune the emission character of the complexes as a function of the remote *para*-substituent of the ancillary ligand.

Conclusions

This paper describes the high-yielding, two-step synthesis of a range of new 5-hydroxyquinoxaline ligands, conveniently utilising a commercially available 2-amino-3-nitrophenol starting material. Variation of the *para*-phenyl substituents provides the means for moderately tuning the electronic characteristics of the ligands. The resultant coordination chemistry yields the first examples of cyclometallated Ir(III) complexes containing functionalised quinoxalinato-based ancillary ligands.

Supporting DFT calculations suggest that both the HOMO and LUMOs are almost completely localised on the coordinated quinoxalinato ligands. Spectroscopically, this facilitates a degree of tuning in the electronic properties of the complexes, whilst the photophysical properties of the complexes appear to be dominated by ligand-centred character at room temperature under ambient conditions.

Experimental

All reactions were performed with the use of vacuum line and Schlenk techniques. Reagents were commercial grade and were used without further purification. $[(ppy)_2Ir(\mu\text{-}Cl)_2Ir(ppy)_2]$ was prepared according to the literature procedure.[15] ^1H and $^{13}C\text{-}\{^1H\}$ NMR spectra were run on NMR-FT Bruker 400 or 250 spectrometers and recorded in $CDCl_3$. ^1H and $^{13}C\text{-}\{^1H\}$ NMR chemical shifts (δ) were determined relative to internal TMS and are given in ppm. Low-resolution mass spectra were obtained by the staff at Cardiff University. High-resolution mass spectra were carried out at the EPSRC National Mass Spectrometry Service at Swansea University. UV-Vis studies were performed on a Jasco V-570 spectrophotometer as MeCN solutions (6.4×10^{-5} M^{-1}). Photophysical data were obtained on a JobinYvon–Horiba Fluorolog spectrometer fitted with a JY TBX picosecond photodetection module as MeCN solutions. Emission spectra were uncorrected and excitation spectra were instrument corrected. The pulsed source was a Nano-LED configured for 372 nm output operating at 500 kHz. Luminescence lifetime profiles were obtained using the JobinYvon–Horiba FluoroHub single photon counting module and the data fits yielded the lifetime values using the provided DAS6 deconvolution software. Quantum yield measurements were obtained on aerated acetonitrile solutions of the complexes, using $[Ru(bpy)_3](PF_6)_2$ in aerated acetonitrile as a standard ($\Phi_{em} = 0.016$).[16] Electrochemical studies were carried out using a Parstat 2273 potentiostat in conjunction with a three-electrode cell. The auxiliary electrode was a platinum wire and the working electrode a platinum (1.0 mm diameter) disc. The reference was a silver wire separated from the test solution by a fine porosity frit and an agar bridge saturated with KCl. Solutions (10 ml CH_2Cl_2) were 1.0×10^{-3} mol dm^{-3} in the test compound and 0.1 mol dm^{-3} in $[NBu^n_4][PF_6]$ as the supporting electrolyte. Under these conditions, $E^{0\prime}$ for the one-electron oxidation of $[Fe(\eta\text{-}C_5H_5)_2]$, added to the test solutions as an internal calibrant, is 0.47 V. Unless specified, all electrochemical values are at $\nu = 200$ mVs^{-1}.

Data collection and processing

Diffraction data for **LH³** and **[Ir(ppy)₂(L²)]** were collected on a Nonius KappaCCD using graphite-monochromated Mo-Kα radiation (λ = 0.71073 Å) at 150 K. Software package Apex 2 (v2.1) was used for the data integration, scaling and absorption correction.

Structure analysis and refinement

The structure was solved by direct methods using SHELXS-97 and was completed by iterative cycles of ΔF-syntheses and full-matrix least squares refinement. All non-H atoms were refined anisotropically and difference Fourier syntheses were employed in positioning idealised hydrogen atoms and were allowed to ride on their parent C-atoms. All refinements were against F^2 and used SHELX-97.[17]

DFT studies

All calculations were performed on the Gaussian 03 program.[18] Geometry optimisations were carried out without constraints using the B3PW91 functional. The LANL2DZ basis set was used for the Ir centres, and was invoked with pseudo-potentials for the core electrons, a 6-31G(d,p) basis set for all coordinating atoms with a 6-31G basis set for all remaining atoms. All optimisations were followed by frequency calculations to ascertain the nature of the stationary point (minimum or saddle point).

Syntheses of the ligands

Ligand LH¹. Zn dust (~1 g) was heated in conc. HCl (15 ml) for 10 min and then added to a solution of 2-amino-3-nitrophenol (0.315 g, 2.04 mmol) in EtOH : HCl (1 M) (1 : 1, 30 ml). The mixture was heated at reflux for 14 h during which time the solution turned from red to pale yellow. The solvents were then removed *in vacuo* and the crude mixture dissolved in EtOH (10 ml). After filtering, benzil (0.340 g, 1.62 mmol) was added and the mixture heated at reflux for 16 h. The solvent was removed *in vacuo* and the black product dissolved in $CHCl_3$ (35 ml). The organic solution was washed with water (2 × 40 ml) and brine (40 ml) and then heated with activated charcoal and $MgSO_4$ for 30 min. The solution was filtered and the solvent removed *in vacuo* to give a yellow crystalline powder. Yield = 0.397 g (1.33 mmol) 82%. ^1H NMR (400 MHz, $CDCl_3$) δ_H = 7.82 (1H, br s), 7.58–7.64 (2H, m), 7.41–7.43 (4H, m), 7.24–7.31 (6H, m), 7.16 (1H, dd, J_{HH} = 6.9 and 1.8 Hz) ppm. $^{13}C\text{-}\{^1H\}$ NMR (101 MHz, $CDCl_3$) δ_C = 154.7, 152.4, 151.5, 141.9, 139.3, 138.9, 131.6, 131.5, 130.3, 130.2,

129.4, 129.3, 128.7, 128.6, 120.0, 111.3 ppm. UV-vis (MeCN): λ_{max} (ε dm^3 mol^{-1} cm^{-1}) = 289 (19600), 350 (6200) nm. AP MS found m/z 299.1, calculated m/z 299.3 for $[M+H]^+$.

Ligand LH^2. Prepared similarly from 2-amino-3-nitrophenol (0.300 g, 1.95 mmol) and 4,4′-dibromobenzil (0.422 g, 1.15 mmol). The product was further purified by column chromatography (silica, CH_2Cl_2) and eluted as the first fraction with CH_2Cl_2. The solvent was removed *in vacuo* to give the product as a yellow crystalline solid. Yield = 0.482 g (1.05 mmol) 93%. ^{1}H NMR (400 MHz, $CDCl_3$) δ_H = 7.62 (2H, m), 7.44 (4H, d, J_{HH} = 8.4 Hz), 7.30 (4H, m), 7.17 (1H, d, J_{HH} = 6.4 Hz) ppm. ^{13}C-{^{1}H} NMR (101 MHz, $CDCl_3$) δ_C = 153.2, 152.3, 149.9, 142.0 137.9, 137.5, 132.9, 132.2, 132.1, 131.8, 131.7, 131.5, 124.3, 124.2, 120.0, 111.8 ppm. UV-vis (MeCN): λ_{max} (ε dm^3 mol^{-1} cm^{-1}) = 294 (16950), 349 (5100) nm. ES MS found m/z 456.9, calculated m/z 457.1 for $[M+H]^+$.

Ligand LH^3. Prepared similarly to **LH^1** from 2-amino-3-nitrophenol (0.540 g, 3.50 mmol) and 4,4′-dimethylbenzil (0.679 g, 2.85 mmol) to give an orange powder. Yield = 0.930 g (2.85 mmol) 100%. ^{1}H NMR (400 MHz, $CDCl_3$) δ_H = 7.65 (1H, d, J_{HH} = 8.4 Hz), 7.58 (1H, br), 7.35 (4H, d, J_{HH} = 8.0 Hz), 7.07 (5H, m), 2.31 (3H, s), 2.28 (3H, s) ppm. ^{13}C-{^{1}H} NMR (101 MHz, $CDCl_3$) δ_C = 154.3, 152.0, 151.2, 141.4 139.1, 139.0, 136.0, 135.7, 131.0, 130.9, 129.8, 129.7, 129.1, 129.0, 119.4, 110.8, 21.4, 21.3 ppm. UV-vis (MeCN): λ_{max} (ε dm^3 mol^{-1} cm^{-1}) = 292 (16450), 355 (7050) nm. EI MS found m/z 326.1, calculated m/z 326.4 for $[M]^+$.

Ligand LH^4. Prepared similarly from 2-amino-3-nitrophenol (0.300 g, 1.95 mmol) and anisil (0.300 g, 1.41 mmol) to give a yellow crystalline solid. Yield = 0.488 g (1.36 mmol) 96%. ^{1}H NMR (400 MHz, $CDCl_3$) δ_H = 7.80 (1H, br), 7.60 (2H, app. quin {coincident dd and d}, J_{HH} = 8.2 Hz), 7.42 (4H, m), 7.13 (1H, d, J_{HH} = 8.0 Hz), 6.81 (4H, d, J_{HH} = 8.2 Hz), 3.78 (3H, s), 3.77 (3H, s) ppm. ^{13}C-{^{1}H} NMR (101 MHz, $CDCl_3$) δ_C = 160.8, 160.7, 154.6, 152.2, 142.8, 142.0, 131.9, 131.7, 131.6, 131.5, 131.3, 131.1, 119.8, 114.3, 114.1, 110.9, 55.8, 55.7 ppm. UV-vis (MeCN): λ_{max} (ε dm^3 mol^{-1} cm^{-1}) = 297 (20000), 364 (9200) nm. ES MS found m/z 359.1, calculated m/z 359.4 for $[M+H]^+$.

Syntheses of the complexes

[Ir(ppy)$_2$(L^1)]. $[(ppy)_2Ir(\mu\text{-}Cl)_2Ir(ppy)_2]$ (0.040 g, 0.037 mmol), **LH^1** (0.023 g, 0.077 mmol) and Na_2CO_3 (0.010 g, 0.094 mmol) were heated at 120 °C in 2-methoxyethanol (10 ml) for 16 h. The solvent was removed *in vacuo* and the crude product dissolved in CH_2Cl_2 (25 ml). The organic solution was washed with water (2 × 25 ml) and brine (25 ml), dried over $MgSO_4$ and filtered. The solvent was lowered in volume (*ca.* 2 ml) *in vacuo* and the product precipitated by the slow addition of Et_2O (20 ml) to give a red solid, which was dried *in vacuo*. Yield = 0.048 g (0.061 mmol) 88%. ^{1}H NMR (400 MHz, $CDCl_3$) δ_H = 8.64 (1H, d, J_{HH} = 5.6 Hz), 7.85 (1H, d, J_{HH} = 5.1 Hz), 7.50–7.69 (6H, m), 7.34 (1H, d, J_{HH} = 7.7 Hz), 6.94–7.14 (9H, m), 6.81 (1H, app. t, J_{HH} = 5.9 Hz){app. = apparent (coincident dd)}, 6.64–6.69 (2H, m), 6.56 (1H, app. t, J_{HH} = 7.6 Hz), 6.39 (1H app. t, J_{HH} = 7.1 Hz), 6.10 (1H, app. t, J_{HH} = 7.3 Hz), 5.82 (1H, d, J_{HH} = 7.1 Hz), 5.49 (1H, d, J_{HH} = 7.6 Hz) ppm. ^{13}C-{^{1}H} NMR (101 MHz, $CDCl_3$) δ_C = 169.5, 168.3, 167.2, 154.6, 151.9, 150.3, 147.9, 147.7, 145.4, 144.2, 142.1, 141.9, 137.9, 135.7, 135.0, 134.1, 132.3, 131.2, 129.9, 128.7, 128.3, 128.2, 128.0, 127.3, 127.0, 126.5, 126.1, 126.0, 122.8, 122.7, 120.8, 120.5, 120.1, 118.1, 118.0, 117.4, 117.1, 111.0 ppm. UV-vis (MeCN): λ_{max} (ε dm^3 mol^{-1} cm^{-1}) = 302 (18050) nm. ES MS found m/z 799.2, calculated m/z 798.9 for $[M+H]^+$. HR MS found m/z 797.2024, calculated m/z 797.2020 for $[C_{42}H_{30}O_1N_4{}^{191}Ir_1]^+$.

[Ir(ppy)$_2$(L^2)]. Prepared similarly from $[(ppy)_2Ir(\mu\text{-}Cl)_2Ir(ppy)_2]$ (0.045 g, 0.042 mmol), **LH^2** (0.038 g, 0.083 mmol) and Na_2CO_3 (0.010 g, 0.094 mmol). Yield = 0.073 g (0.076 mmol) 91%. ^{1}H NMR (400 MHz, $CDCl_3$) δ_H = 8.61 (1H, d, J_{HH} = 5.6 Hz), 7.54–7.77 (6H, m), 7.36 (1H, d, J_{HH} = 7.7 Hz), 7.17–7.20 (4H, m), 7.10 (1H, d, J_{HH} = 8.1 Hz), 6.95–7.02 (2H, m), 6.89 (2H, 2 × d, J_{HH} = 8.2 Hz), 6.81 (1H app. t, J_{HH} = 5.9 Hz), 6.32–6.71 (6H, m), 6.25 (1H, app. t, J_{HH} = 7.6 Hz), 5.80 (1H, d, J_{HH} = 7.6 Hz), 5.49 (1H, d, J_{HH} = 7.6 Hz) ppm. ^{13}C-{^{1}H} NMR (101 MHz, $CDCl_3$) δ_C = 171.1, 169.2, 168.7, 154.4, 151.5, 150.7, 150.0, 149.4, 148.9, 146.4, 145.8, 143.5, 143.2, 137.9, 137.4, 137.3, 136.6, 134.6, 134.3, 132.7, 131.5, 131.4, 131.2, 130.9, 130.3, 130.2, 124.5, 124.4, 123.8, 123.4, 122.3, 122.1, 121.7, 119.7, 119.6, 119.3, 118.7, 112.5 ppm. UV-vis (MeCN): λ_{max} (ε dm^3 mol^{-1} cm^{-1}) = 302 (16650) nm. ES MS found m/z 957.0, calculated m/z 956.7 for $[M+H]^+$. HR MS found m/z 953.0235, calculated m/z 953.0230 for $[C_{42}H_{28}O_1N_4Br_2{}^{191}Ir_1]^+$.

[Ir(ppy)$_2$(L^3)]. Prepared similarly from $[(ppy)_2Ir(\mu\text{-}Cl)_2Ir(ppy)_2]$ (0.048 g, 0.045 mmol), **LH^3** (0.031 g, 0.094 mmol) and Na_2CO_3 (0.010 g, 0.094 mmol). Yield = 0.065 g (0.079 mmol) 93%. ^{1}H NMR (400 MHz, $CDCl_3$) δ_H = 8.62 (1H, d, J_{HH} = 5.6 Hz), 7.84 (1H, d, J_{HH} = 5.7 Hz), 7.47–7.68 (6H, m), 7.33 (1H, d, J_{HH} = 7.6 Hz), 7.11 (2H, 2 × d, J_{HH} = 8.0 Hz), 6.90–6.99 (5H, m), 6.75–6.83 (3H, m), 6.67 (1H, app. t, J_{HH} = 7.5 Hz), 6.56 (1H app. t, J_{HH} = 7.5 Hz), 6.47 (1H, app. t, J_{HH} = 7.6 Hz), 6.24 (2H, br), 6.11 (1H, app. t, J_{HH} = 7.6 Hz), 5.83 (1H, d, J_{HH} = 7.5 Hz), 5.45 (1H, d, J_{HH} = 7.6 Hz), 2.14 (3H, s), 1.96 (3H, s) ppm. ^{13}C-{^{1}H} NMR (101 MHz, $CDCl_3$) δ = 169.5, 168.0, 167.2, 159.3, 154.4, 152.0, 149.7, 147.9, 147.7, 147.6, 145.3, 144.3, 142.1, 141.9, 136.9, 136.5, 135,5, 135.1, 134.9, 132.0, 131.9, 131.3, 129.8, 128.6, 128.3, 127.9, 127.8, 127.3, 127.0, 122.7, 122.6, 120.8, 120.4, 120.0, 118.0, 117.3, 117.1, 111.0, 20.3, 20.1 ppm. UV-vis (MeCN): λ_{max} (ε dm^3 mol^{-1} cm^{-1}) = 294 (14450) nm. ES MS found m/z 827.3 and 890.3, calculated m/z 827.0 and 890.0 for $[M+H]^+$ and $[M+MeCN+Na]^+$ respectively. HR MS found m/z 825.2329, calculated m/z 825.2333 for $[C_{44}H_{34}O_1N_4{}^{191}Ir_1]^+$.

[Ir(ppy)$_2$(L^4)]. Prepared similarly from $[(ppy)_2Ir(\mu\text{-}Cl)_2Ir(ppy)_2]$ (0.045 g, 0.042 mmol), **LH^4** (0.032 g, 0.089 mmol) and Na_2CO_3 (0.010 g, 0.094 mmol). Yield = 0.069 g (0.080 mmol) 96%. ^{1}H NMR (400 MHz, $CDCl_3$) δ_H = 8.63 (1H, d, J_{HH} = 5.1 Hz), 7.82 (1H, d, J_{HH} = 5.1 Hz), 7.48–7.67 (5H, m), 7.32 (1H, d, J_{HH} = 6.9 Hz), 7.15 (1H, d, J_{HH} = 7.8 Hz), 7.10 (1H, d, J_{HH} = 8.0 Hz), 6.93–6.99 (4H, m), 6.77 (1H, app. t, J_{HH} = 7.2 Hz), 6.66 (1H, app. t, J_{HH} = 7.5 Hz), 6.53–6.58 (3H m), 6.44 (1H, app. t, J_{HH} = 8.0 Hz), 6.17 (1H, app. t, J_{HH} = 7.6 Hz), 6.02 (2H, br), 5.82 (1H, d, J_{HH} = 7.6 Hz), 5.53 (1H, d, J_{HH} = 6.9 Hz), 3.62 (3H, s), 3.56 (3H, s) ppm. ^{13}C-{^{1}H} NMR (101 MHz, $CDCl_3$) δ_C = 168.9, 167.3, 166.5, 157.7, 156.9, 153.4, 151.1, 149.5, 147.9, 147.3, 146.9, 144.8, 143.6, 141.5, 135.0, 134.3, 131.5, 130.8, 129.8, 129.3, 129.2, 128.6, 128.0, 127.2, 126.9, 122.1, 121.9, 120.2, 119.8, 119.5, 117.4, 117.2, 116.4, 116.3, 111.4, 111.1, 110.3, 53.5, 53.0 ppm. UV-vis (MeCN): λ_{max} (ε dm^3 mol^{-1} cm^{-1}) = 286 (14450) nm. ES MS found

m/z 859.2, calculated *m/z* 859.0 for $[M+H]^+$. HR MS found *m/z* 857.2234, calculated *m/z* 857.2231 for $[C_{44}H_{34}O_3N_4{}^{191}Ir_1]^+$.

Acknowledgements

The EPSRC are thanked for funding. Dr Robert Jenkins, Mr Robin Hicks and Mr David Walker are thanked for running low resolution mass spectra. The staff of the EPSRC MS National Service at the University of Swansea are also gratefully acknowledged.

Notes and references

1 (*a*) C. W. Tang and S. A. VanSlyke, *Appl. Phys. Lett.*, 1987, **51**, 913; (*b*) *Organic Light-Emitting Diodes*, ed. K. Müllen and U. Scherf, Wiley-VCH, Weinheim, 2006.

2 (*a*) J. Luo, C. Yang, J. Zheng, J. Ma, L. Liang and M. Lu, *Eur. Polym. J.*, 2011, **47**, 385; (*b*) P. J. Jadhav, B. N. Limketkai and M. A. Baldo, *Adv. Polym. Sci.*, 2010, **223**, 29; (*c*) J. L. Serrano, L. Garcia, J. Perez, E. Perez, J. M. Galiana, J. Garcia, M. Martinez, G. Sanchez and I. de Silvia, *Dalton Trans.*, 2011, **40**, 156; (*d*) P. Conelly-Espinosa and D. Morales-Moralez, *Inorg. Chim. Acta*, 2010, **363**, 1311; (*e*) F. Cheng and F. Jäkle, *Chem. Commun.*, 2010, **46**, 3717; (*f*) H. Li and F. Jäkle, *Macromolecules*, 2009, **42**, 3448.

3 E. Baranoff, J-H. Yum, M. Grätzel and Md. K. Nazeeruddin, *J. Organomet. Chem.*, 2009, **694**, 2661.

4 (*a*) I-S. Shin, H-C. Lim, J-W. Oh, J-K. Lee, T. H. Kim and H. Kim, *Electrochem. Commun.*, 2011, **13**, 64; (*b*) H-C. Su, Y-H. Lin, C-H. Chang, H-W. Lin, C-C. Wu, F-C. Fang, H-F. Chen and K-T. Wong, *J. Mater. Chem.*, 2010, **20**, 5521; (*c*) L. He, L. Duan, J. Qiao, G. Dong, L. Wang and Y. Qiu, *Chem. Mater.*, 2010, **22**, 3535; (*d*) C. Rothe, C-J. Chiang, V. Jankus, K. Abdullah, X. Zeng, R. Jitchati, A. S. Batsanov, M. R. Bryce and A. P. Monkman, *Adv. Funct. Mater.*, 2009, **19**, 2038; (*e*) S. Graber, K. Doyle, M. Neuburger, C. E. Housecroft, E. C. Constable, R. D. Costa, E. Orti, D. Repetto and H. J. Bolink, *J. Am. Chem. Soc.*, 2008, **130**, 14944.

5 E. Baranoff, J-H. Yum, I. Jung, R. Vulcano, M. Grätzel and Md. K. Nazeeruddin, *Chem.–Asian J.*, 2010, **5**, 496.

6 V. Fernández-Moreira, F. L. Thorp-Greenwood and M. P. Coogan, *Chem. Commun.*, 2010, **46**, 186.

7 (*a*) A. Curioni, M. Boero and W. Andreoni, *Chem. Phys. Lett.*, 1998, **294**, 263; (*b*) M. D. Halls and H. B. Schlegel, *Chem. Mater.*, 2001, **13**, 2632; (*c*) J. Zhang and G. Frenking, *J. Phys. Chem. A*, 2004, **108**, 10296; (*d*) P. E. Burrows, Z. Shen, V. Bulovic, D. M. McCarty, S. R. Forrest, J. A. Cronin and M. E. Thompson, *J. Appl. Phys.*, 1996, **79**, 7991.

8 (*a*) T. Tsuboi, S. Polosan, D-F. Huang and T. J. Chow, *Thin Solid Films*, 2008, **516**, 2788; (*b*) V. A. Montes, R. Pohl, J. Shinar and P. Anzenbacher Jr, *Chem.–Eur. J.*, 2006, **12**, 4523.

9 (*a*) S. Kappaun, S. Eder, S. Sax, R. Saf, K. Mereiter, E. J. W. List and S. Slugovc, *J. Mater. Chem.*, 2006, **16**, 4389; (*b*) S. Kappaun, S. Sax, S. Eder, K. C. Möller, K. Waich, F. Niedermair, R. Saf, K. Mereiter, J. Jacob, K. Müllen, E. J. W. List and C. Slugovc, *Chem. Mater.*, 2007, **19**, 1209; (*c*) C. Yi, C-J. Yang, J. Liu, M. Xu, J-H Wang, Q-Y. Cao and X-C. Gao, *Inorg. Chim. Acta*, 2007, **360**, 3493; (*d*) N. Agarwal and P. K. Nayak, *Tetrahedron Lett.*, 2008, **49**, 2710; (*e*) S. Polosan, T. J. Chow and T. Tsuboi, *J. Phys. Org. Chem.*, 2008, **21**, 315.

10 (*a*) E. S. Lane, *Analyst*, 1955, **80**, 675; E. S. Lane and C. Williams, *J. Chem. Soc.*, 1956, 2983; (*b*) J. Nasielski, S. Heilporn, R. Nasielski-Hinkins and F. Geerts-Evrard, *Tetrahedron*, 1987, **43**, 4329; (*c*) J. Nasielski, S. Heilporn, E. Chauveheid, K. Poppe and R. Nasielski-Hinkins, *Bull. Soc. Chim. Belg.*, 1990, **99**, 783; (*d*) H-S. Lin and M. E. Richet, *PCT Int. Appl.*, 1999, WO9952365; (*e*) W. Wrasidlo, J. Doukas, I. Royston, G. Noronha, J. D. Hood, E. Dneprovskaia, X. Gong, U. Splittgerber and N. Zhao, *PCT Int. Appl.*, 2004, WO2004030635.

11 (*a*) A. J. Hallett, B. D. Ward, B. M. Kariuki and S. J. A. Pope, *J. Organomet. Chem.*, 2010, **695**, 2401; (*b*) S. Lamansky, P. Djurovich, D. Murphy, F. Abdel-Razzaq, R. Kwong, I. Tsyba, M. Bortz, B. Mui, R. Bau and M. E. Thompson, *Inorg. Chem.*, 2001, **40**, 1704.

12 L-L. Shi, Y. Geng, H-Z. Gao, Z-M. Su and Z-J. Wu, *Dalton Trans.*, 2010, **39**, 7733.

13 (*a*) A. Mishra, P. K. Nayak, D. Ray, M. P. Patankar, K. L. Narasimhan and N. Periasamy, *Tetrahedron Lett.*, 2006, **47**, 4715; (*b*) B. W. D. Andrade, S. Datta, S. R. Forrest, P. Djurovich, E. Polikarpov and M. E. Thompson, *Org. Electron.*, 2005, **6**, 11.

14 S. Kappaun, S. Eder, S. Sax, K. Mereiter, E. J. W. List and C. Slugovc, *Eur. J. Inorg. Chem.*, 2007, 4207.

15 M. Nonoyama, *Bull. Chem. Soc. Jpn.*, 1974, **47**, 767.

16 (*a*) M. Frank, M. Nieger, F. Vogtle, P. Belser, A. von Zelewsky, L. D. Cola, V. Balzani, F. Barigelletti and L. Flamigni, *Inorg. Chim. Acta*, 1996, **242**, 281; (*b*) A. Juris, V. Balzani, F. Barigelletti, S. Campagna, P. Belser and A. Von Zelewsky, *Coord. Chem. Rev.*, 1988, **84**, 85.

17 *SHELXL-PC Package*, Bruker Analytical X-ray Systems, Madison WI, 1988.

18 M. J. Frisch, G. W. Trucks, H. B. Schlegel, G. E. Scuseria, M. A. Robb, J. R. Cheeseman, J. A. Montgomery Jr., T. Vreven, K. N. Kudin, J. C. Burant, J. M. Millam, S. S. Iyengar, J. Tomasi, V. Barone, B. Mennucci, M. Cossi, G. Scalmani, N. Rega, G. A. Petersson, H. Nakatsuji, M. Hada, M. Ehara, K. Toyota, R. Fukuda, J. Hasegawa, M. Ishida, T. Nakajima, Y. Honda, O. Kitao, H. Nakai, M. Klene, X. Li, J. E. Knox, H. P. Hratchian, J. B. Cross, V. Bakken, C. Adamo, J. Jaramillo, R. Gomperts, R. E. Stratmann, O. Yazyev, A. J. Austin, R. Cammi, C. Pomelli, J. W. Ochterski, P. Y. Ayala, K. Morokuma, G. A. Voth, P. Salvador, J. J. Dannenberg, V. G. Zakrzewski, S. Dapprich, A. D. Daniels, M. C. Strain, O. Farkas, D. K. Malick, A. D. Rabuck, K. Raghavachari, J. B. Foresman, J. V. Ortiz, Q. Cui, A. G. Baboul, S. Clifford, J. Cioslowski, B. B. Stefanov, G. Liu, A. Liashenko, P. Piskorz, I. Komaromi, R. L. Martin, D. J. Fox, T. Keith, M. A. Al-Laham, C. Y. Peng, A. Nanayakkara, M. Challacombe, P. M. W. Gill, B. Johnson, W. Chen, M. W. Wong, C. Gonzalez and J. A. Pople, *Gaussian 03*, Revision E.01, Gaussian Inc, Wallingford CT, 2004.